Final Report: Sintered CZTS Nanoparticle Solar Cells on Metal Foil

July 26, 2011 — July 25, 2012

Craig Leidholm, Charlie Hotz, Alison Breeze, Chris Sunderland, Wooseok Ki, and Don Zehnder
Solexant Corp.
San Jose, California

NREL Technical Monitor: Brian Keyes

Final Report: Sintered CZTS Nanoparticle Solar Cells on Metal Foil

July 26, 2011 — July 25, 2012

Craig Leidholm, Charlie Hotz, Alison Breeze, Chris Sunderland, Wooseok Ki, and Don Zehnder
Solexant Corp.
San Jose, California

NREL is a national laboratory of the U.S. Department of Energy, Office of Energy Efficiency & Renewable Energy, operated by the Alliance for Sustainable Energy, LLC.

Table of Contents

List of Figures

List of Tables

1 Summary

This is the final report covering 12 months of this subcontract for research on high-efficiency copper zinc tin sulfide (CZTS)-based thin-film solar cells on flexible metal foil. Each of the first three quarters of the subcontract has been detailed in quarterly reports. In this final report highlights of the first three quarters will be provided and details will be given of the final quarter of the subcontract.

Major accomplishments for the one-year subcontract include:

Quarter 1:

- Successfully demonstrated the controlled and repeatable synthesis of nanoparticles (NPs) for deposition by standard drawdown techniques.

- Achieved controllable synthesis of NPs with several compositions and using various synthesis routes

- Synthesized NPs of both CZTS and copper zinc tin selenide (CZTSe)

- Accomplished uniform and repeatable draw-down coating of the formulated inks onto Mo-coated foil substrates

- Fabricated thin-film absorbers of various S/Se concentrations and resulting bandgaps from 1.0 to 1.1.

- Achieved 8.1% solar cell, surpassing ahead of schedule the 5% and 7% small-area cell deliverables for this quarter.

- Collaborated with NREL researchers Manuel Romero and Mowafak Al-Jassim to measure electronic properties by cathodoluminescence (CL) and Electron-Beam Induced Current (EBIC).

Quarter 2:

- Achieved high compositional reproducibility and size distribution of 150ml scaled CZTS ink batch

- Fabricated devices using mixtures of CZTS and CZTSe ink

- Synthesized NPs of controllably mixed sulfur and selenium composition ($CZTS_xSe_{1-x}$)

- NPs were synthesized from alternative Cu, Zn and Sn sources

- Collaborated with the NREL scanning transmission electron microscopy high angle annular dark field (STEM-HAADF) facilities to measure the intra-particle elemental composition variability and NREL's Steve Johnston to investigate root causes of shunting using drive level infrared thermography (DLIT)

- Achieved 9.7% solar cell (internal measurement) and succeeded in meeting the 9% small-area cell subcontract deliverable

All figures in this report are property of Solexant.

Quarter 3:

- Achieved 10.2% (internal measurement), 9.85% NREL measured small area cell, meeting the 10% small-area cell subcontract deliverable within experimental uncertainty.

- Achieved 6.7% large-area cells (25mmx25mm)

- Formulated ink for higher viscosity suitable for printing on Solexant's wide-width print tool

- Comparatively studied the grain growth and cell performance of cells made with NPs synthesized using 4 different surfactants

Quarter 4:

- Achieved 8.3% large area cell (25mmx25mm)

- Successfully printed 10 meters of continuous wide-width web with CZTS ink, and fabricated >6% small area cells on 5 sections across the width of the web

- Achieved 7.1% efficient $25cm^2$ mini-module (internal measurement)

2 Introduction

Background

This final report covers the one-year effort under an NREL PV Technology Incubator Tier 1 subcontract with Solexant Corporation which supports the materials development and solar cell fabrication studies on CZTSSe thin-film materials.

Technical Approach

NP Printed Absorber

Roll-to-roll printed CZTS nanoparticle technology provides the combination of fast, atmospheric pressure deposition, a lightweight substrate, and a thin, inexpensive absorber layer, each of which decrease the cost of the final installed module. Our objective for this project was to validate the use of CZTSSe absorber in manufacturable, high efficiency solar cells. The ultimate goal of this effort is to fabricate CZTSSe solar cells on flexible stainless steel (SS) substrates. The device structure implemented is similar to the well-established CIGS device structure, namely molybdenum (Mo) back contact, cadmium sulfide (CdS) window layer and zinc oxide (ZnO)/ aluminum-doped zinc oxide (AZO) bi-layer transparent conducting oxide (TCO) stack as top contact. The nature of the reactive selenization process used in this work required improvement of the back contact Mo as well as the underlying barrier layer to prevent contaminants diffusing from the stainless steel (SS) substrate. The CdS window layer was deposited by the common chemical bath deposition (CBD) technique.

Absorber Formation

For absorber formation, we used two reaction systems; a traditional tube furnace and an RTP system. The tube furnace configuration is a well-understood process tool for controllable selenization of precursor materials. This process was the initial foundation for establishing CZTSSe absorber materials with reasonable grain growth and resulted in cells up to 10%.

However the lengthy thermal process used in that tool is not viewed as a commercially scalable process, primarily due to its extended process time. Therefore the effort to use an RTP process was launched at the beginning of the project in order to develop a faster absorber formation process for eventual transfer to Solexant's pilot process line.

Characterization Tools

Solexant has an array of analytical tools in-house that were used extensively throughout this project effort. These tools include scanning electron microscopy (SEM), transmission electron microscopy (TEM), electron beam induced current (EBIC), electron dispersive spectroscopy (EDS), white-light interferometry, Infrared Thermography, optical absorption spectroscopy, x-ray fluorescence (XRF), capacitance-voltage (C-V), current-voltage (I-V) and light-biased quantum efficiency (QE). We had collaborative efforts with NREL's Measurement and Characterization group for lock-in Infrared Thermography, SEM, focused ion beam (FIB)-SEM and EDS, STEM, EBIC, cathodoluminescence (CL) and Raman.

3 Overall Development Details

Summary of Accomplishments during Subcontract Q1 thru Q3

Quarter 1

The technical objectives included in quarter 1 were to develop methods to synthesize nanoparticles (NPs) for CZTSSe absorber film formation and then, using the NPs, develop thermal methods and processes for forming high-quality absorber layers and fabricate solar cells using these absorber layers. All layer deposition and formation and device fabrication were performed on Solexant's standard flexible stainless steel foil substrates.

In the first quarter of work, we successfully demonstrated the controlled and repeatable synthesis of NPs for deposition by standard drawdown techniques. In particular the NP/ink group established a baseline synthesis method from which other studies could be compared.

For the baseline NP synthesis process, a hot-injection method using oleylamine was selected and CZTS NPs with diameter on the order of 5-10nm were controllably produced in milliliter-scale batches (Figure 1). Additional XRD analysis indicates the material to be relatively uniform and crystalline, proving reasonable particle-to-particle compositional uniformity. With the baseline synthesis method in place, Cu/(Zn+Sn) compositions ranging from 0.65 to 0.95 were produced to compare grain growth and cell performance.
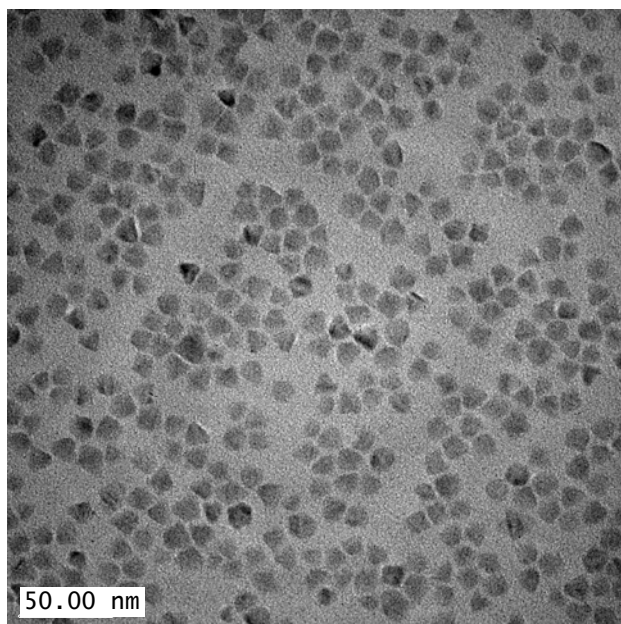
Figure 1 - TEM micrograph of Solexant's CZTS synthesized nanoparticles.

Early cell results showed that selenide absorber layers formed by more extensive selenization of the CZTS printed layers outperformed their sulfide counterparts. Therefore in an effort to affect the thermodynamics of CZTSe film formation, CZTSe NPs were synthesized. These proved to be more challenging than the sulfides due to reactivity differences between the sulfur and selenium in the synthesis process.

Published work on CZTSSe cells show that, similar to CIGS, the Group I to Group II and IV (Cu/Zn+Sn) significantly affect the electronic properties of the absorber material. Additionally researchers report a difficulty in controlling the loss of Sn during thermal processes due to the high vapor pressure of SnS. As our approach differed from others, we investigated a wide range of compositions, both Cu/(Zn+Sn) and Zn/Sn to understand our process sensitivity to these variables. Interestingly the process developed showed a relatively wide range of acceptable compositions, from approximately 0.75 to 0.95, although 0.8 and 1.2 for the Cu/(Zn+Sn) and Zn/Sn, respectively, gave the most repeatable and best efficiency cells.

The initial electrode stack used in this work was a metallic diffusion barrier layer deposited onto stainless steel substrates followed by a 500-1000 nm molybdenum back-contact layer. The CZTS NP solutions were then coated directly onto the molybdenum thin-film layer using the cup-coating, drawdown technique. In this work most absorber layers fabricated were from multiple printed layers rather than a single layer. Solexant has found throughout the work in printed NP layers that multiple layers provides some advantages of single layers including filling and repairing voids and defects in any one layer. By controlling the drying conditions and atmosphere during the print/dry step, the interfaces between printed layers is indiscernible in the final absorber films. Typical printed layer thickness was 250nm per print, allowing 6 to 8 successive printed layers to achieve the 1.5 to 2.0 microns target thickness. All printing and drying of layers was performed in a nitrogen glovebox with ppm O_2 levels. Each layer requires drying to "cure" the layer and prevent dissolution of existing printed layers in subsequent printed

layers. Typical drying temperatures between 300 and 400C were performed in the glovebox between each layer using a basic hot plate. While the printing step is likely able to be performed in a normal air environment, the drying/curing step needs to be done in a low-O_2 environment to prevent oxidation of each layer. For production this would require a commercially available controlled-environment belt furnace for this step, a relatively low-cost tool.

A significant portion of the work during the first quarter was the development of the thermal processing of the printed layers to form high-quality absorber layers. The temperatures for the thermal process that gave the best results were similar to other published reports, namely in the range of 500-550°C. During this period we also adjusted the thermal environment with different reactive species including sulfur and selenium. It was found that the films that achieved the largest-grained materials were obtained when a selenium partial pressure was provided during the thermal treatment. The final absorber films, therefore, include selenium and thus are lower band gap than pure CZTS. By adjusting the selenium partial pressure and the time and temperature of the thermal anneal, the amount of "selenization" of the film was able to be controlled. Through this initial phase the best devices were formed using more thoroughly selenized films, with band gaps in the range of 1.0 to 1.05 eV.

The junction was completed using CBD CdS to a thickness between 30 and 40nm. The process used is the common sulfate chemistry process with bath temperatures in the range of 65-80°C with deposition times typically 6-10 minutes.

The devices were completed with commonly-used ZnO/AZO stacks and Ni/Al evaporated contact grids. Some development was necessary on the grids as this process was not part of Solexant's baseline process. The grid development process exposed a defect in the devices that caused degraded device performance compared to performance without grids. The cause of the degraded performance turned out to be iron-selenide defects caused by selenium reaching the SS substrate through defects in the barrier layer. The small-area cells were not affected as the high resistivity CdS and i-ZnO layers provide a level of electrical screening from these low-resistance shunt paths. However the grid increases the statistical likelihood of touching one of these defects and reduces the effective screening by the window layers. This issue of iron-selenide defect formation continued to challenge us throughout the duration of this project and was the primary cause of poor performance of large-area (25mmx25mm) cells fabricated in quarters 3 and 4.

The Solexant team achieved impressive early results of small-area cell efficiencies greater than 8%. The device efficiency curve of a typical cell from the six (6) cells measured at NREL is shown below.

Solexant

CZTS Cell

Device ID: 993002AE-2   Device Temperature: 24.8 ± 0.5 °C
Aug 31, 2011 12:35   Device Area: 0.2464 cm^2
Spectrum: ASTM G173 global   Irradiance: 1000.0 W/m^2

NREL   X25 IV System
              PV Performance Characterization Team
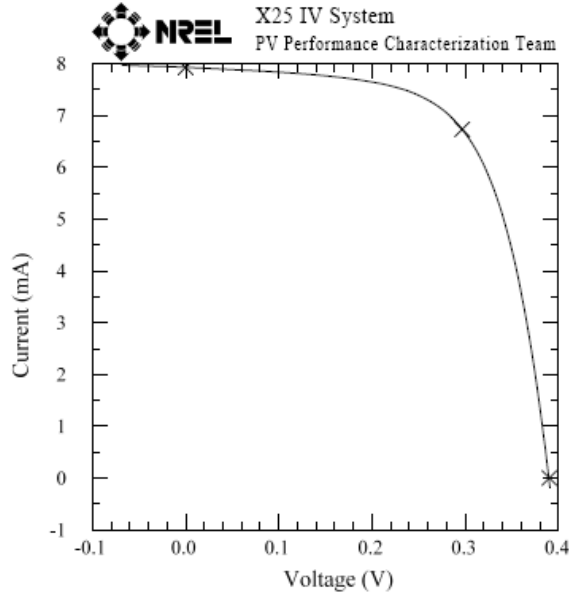
V_{oc} = 0.3903 V I_{max} = 6.7337 mA
I_{sc} = 7.9302 mA V_{max} = 0.2970 V
J_{sc} = 32.184 mA/cm^2 P_{max} = 1.9997 mW
Fill Factor = 64.60 %   Efficiency = 8.12 %

Figure 2 - NREL Light I-V measurement of cell submitted for Q1 milestone.

One additional challenge faced in the NP-based CZTSSe absorber layers was the grain structure of selenized films which exhibited a tri-layer morphology. This is believed to be due to a nucleation that occurs from both bottom and top of the printed layer, leaving a small-grained material sandwiched between two crystalline layers. Because of this structure, only the top crystalline portion contributes to photoresponse of the device. As this is clearly undesirable, we worked to understand the thermodynamics of the thermal process. Amazingly cells better than 8% were fabricated on a regular basis even early on, suggesting that the performance of the thin (~800nm) top layer was exemplary. To help understand fundamental electronic performance parameters, Solexant collaborated with NREL researchers Manuel Romero and Mowafak Al-Jassim to measure electronic properties by cathodoluminescence (CL) and Electron-Beam Induced Current (EBIC). The EBIC scan showed remarkably uniform photoresponse across the thickness of the top layer. This data gave us hope that notably higher efficiencies could be achieved if this tri-layer morphology could be eliminated and, therefore, the elimination of the tri-layer became a significant focus of development in the remaining three quarters of the subcontract.
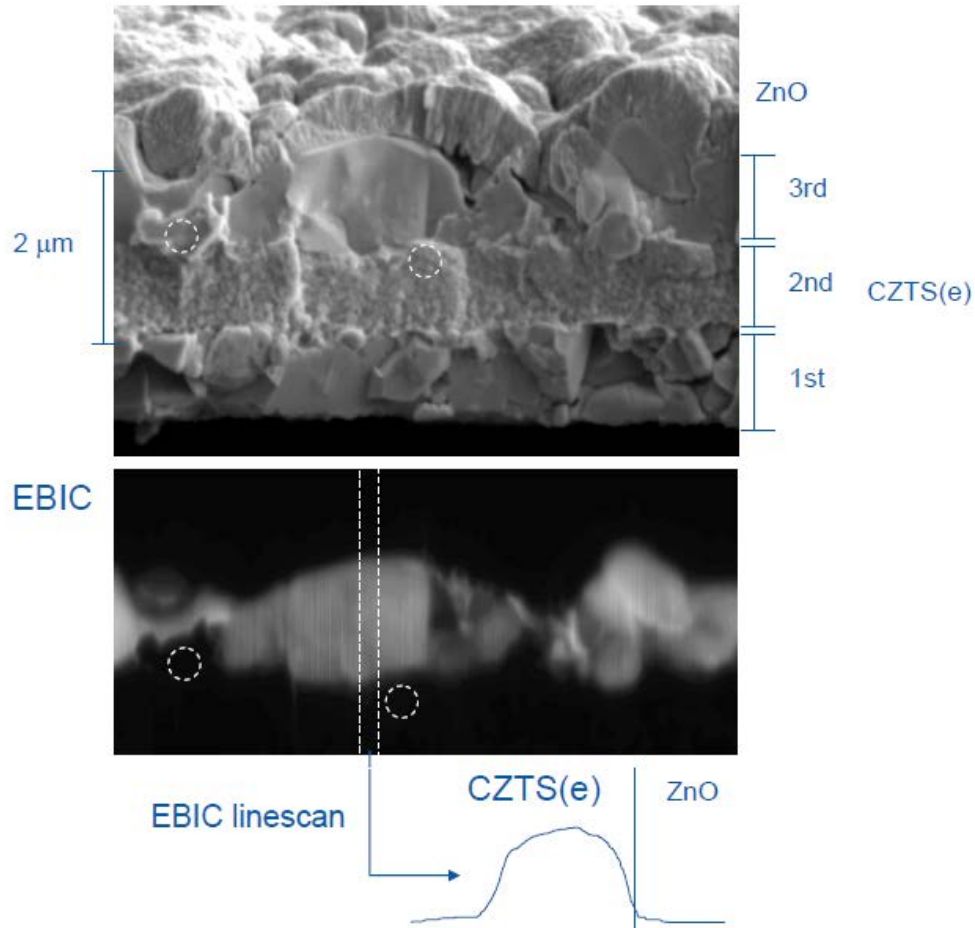
Figure 3 - EBIC image of CZTSSe device.

Quarter 2

In the second quarter of the project, we continued to look at thermodynamics of the absorber formation, back contact improvement and scaling of the baseline NP synthesis and ink formulation for printing on the full-width pilot printing tool.

Additionally, being that the reactive anneal is performed in a high-selenium-concentration atmosphere, we worked to develop a back contact that could withstand the thermal process without delamination due to full selenization of that layer. We were successful in creating a Mo-based back contact that was still partially reactive with Se to form the helpful p-type Mo_xSe layer for good ohmic back contact.

As far as ink scaling, we required an approximate 50-fold scale increase to produce enough NPs and subsequent ink to print multiple meters on the 750mm wide pilot tool.

NP and Ink Development

By the end of the contract, a goal was to print 10 meters of continuous wide-width web with CZTS ink and fabricate better than 4% cells from multiple locations across the web. Toward that

effort the NP synthesis and ink formulation needed to be scaled by at least 50 times. Additionally the rheology needed to be adjusted to properly print using the existing pilot tooling but this was done following successful completion of the scale-up process in this quarter. CZTS ink was scaled to the 150 mL scale (~10x initial batch size), adequate to print 1-2 meters of web on Solexant's pilot production tool and multiple back-to-back NP synthesis batches showed repeatable particle size distribution and composition. The resulting inks were used to fabricate small-area devices to further qualify the NP ink and were successful in demonstrating similar efficiencies as cells fabricated using the now baseline CZTS ink. This was a substantial achievement to demonstrate scalability toward eventual liter-batch size ink production to be used in the wide-web printing development later in this subcontract.

In the first quarter Solexant synthesized NPs of both CZTS and CZTSe composition and tested cells fabricated from each. During the second quarter, in order to further explore the material territory between these two cases, inks of mixed S and Se content were synthesized. By control of sulfur and selenium reagent ratio, nanoparticles of 30% and 50% selenium content were synthesized while maintaining the Cu/(Zn+Sn) and Zn/Sn ratios previously found to be an optimal range for the most efficient CZTSSe devices. Interestingly, while devices weren't notably worse than those made from the standard, they also did not outperform them. In short no net benefit was identified, although this route provides some options as the development work moves in the direction of alternate buffer layers.

Multiple inks were prepared aimed at determining if any aspect of the synthetic strategy pursued in the production of the nanoparticle ink is limiting device efficiency. Inks were synthesized from alternative Cu, Zn and Sn sources and also using different surfactants. Additionally, some inks were modified post-synthesis to change and reduce the surfactant content. All inks were examined for printing and selenization behavior and some were carried through to device fabrication. No significant device performance improvement versus controls was observed for the inks that were processed through to devices. This indicates the ink did not have a clear performance problem that would lead us to pursue another synthetic process. However, testing alternate ink compositions and formulations continued throughout the balance of this project.

In conjunction with the NREL STEM-HAADF facilities (Andrew Norman and Mowafak Al-Jassim), a measurement of the intra-particle elemental composition variability was obtained. The results indicate that there is a significant particle-to-particle variation in the Cu:Zn:Sn metal ratios. This was not unexpected given the nature of the synthesis, prior results from XRD and literature results. It does clearly eliminate the possibility that the inks are a mixture of binaries, or of Cu_2SnS_3 and ZnS. The significance of these results to eventual device performance is not clear as a mixture of heterogeneous particles at the nanometer scale may not be functionally different (after device fabrication) from an ink composed of homogeneous particles.
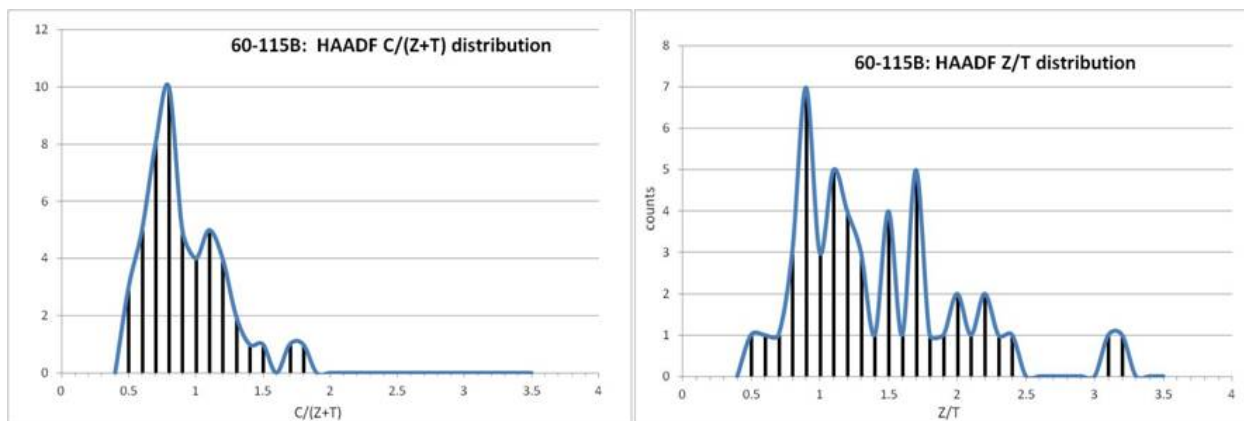
Figure 4 - Scanning TEM Cu/Zn/Sn composition results across representative NP sample.

Films/Devices

Continued refinement to our absorber layer and thermal processing (time, temperature ramp rate and selenium concentration) has yielded improved efficiency devices. Solexant in-house measurement under AM1.5G conditions showed performance up to 9.7% as shown below. This and two other devices were submitted for NREL measurement to fulfill the second quarter 9% device deliverable requirement.
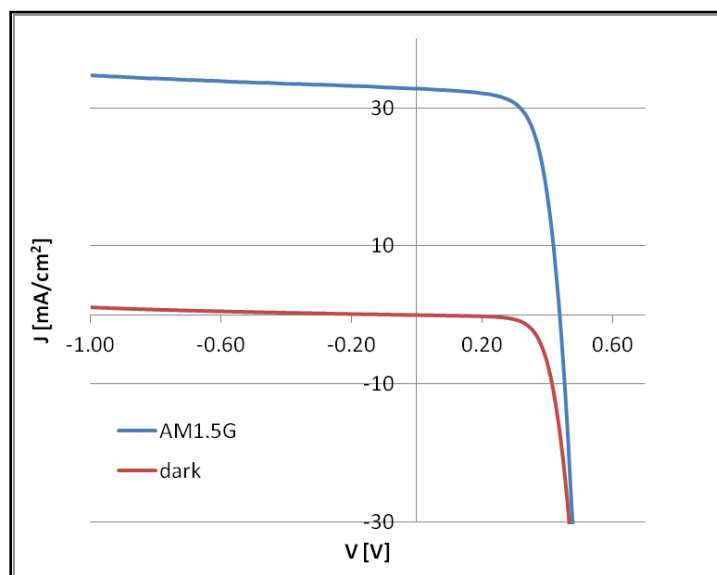
Figure 5 - Solexant in-house measurement of a device submitted to NREL as part of the 9% deliverable requirement.

Inductively coupled plasma mass spectroscopy (ICP-MS) characterization comparing our absorber material before and after selenization has shown that Sn is lost during the thermal treatment, consistent with various literature reports. However devices continued to perform well, typically 8-9%. This suggests that, even with the higher ending ratio Cu/(Zn+Sn) ~ 0.95) the electronic properties of the absorber are conducive to good photoresponse. However to explore possible improvements in cell performance, the addition of Sn-containing NPs to baseline ink formulations via various compounds was explored. Additionally mitigation of Sn loss during

thermal processing was attempted by the addition of Sn compounds in the anneal environment during the reactive thermal treatment.

In the former case it is hoped that providing additional Sn in the precursor would compensate for some of the loss. In the latter experiment, the motivation was to provide an overpressure of Sn to prevent the Sn loss during treatment. For the standard thermal anneal process, the device performance was negatively impacted in each case. Sn compound nanoparticles blended into the precursor ink and the Sn compound included during thermal treatment each yielded somewhat lower than standard efficiency, while elemental Sn included during thermal treatment resulted in very poor devices. In the latter case we believe the Sn reacted with the Se to create SnSe, thus starving the thermal anneal environment of sufficient reactive Se.
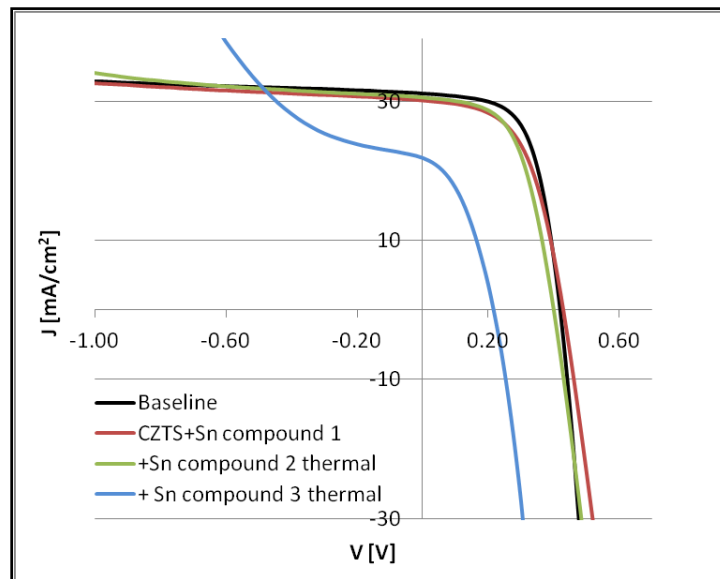
Figure 6 - Results of approaches attempting to address Sn loss during thermal treatment.

Table 1 – Cell performance when fabricated on absorbers with different methods to address Sn loss during thermal treatment

	V_{oc} [V]	J_{sc} [mA/cm^2]	FF [%]	η [%]
Baseline	0.42	31.1	61.2	7.99
CZTS+Sn compound 1	0.43	30.1	55.2	7.12
+Sn compound 2 thermal	0.40	30.5	56.3	6.86
+ Sn compound 3 thermal	0.22	21.8	40.4	1.90

The thickness of the absorber layer was varied both thinner and thicker than the standard value to both optimize efficiency as well as provide insight into performance limitations. The thickest absorber resulted in lower performance due to increased series resistance. Interestingly, the thinnest active layer showed improved long wavelength collection as well as an apparent band gap shift. Based on the EQE measurement of these devices (Figure 7) this is attributed to the baseline thermal treatment creating different S:Se ratios in the final absorber for different absorber thicknesses.

Table 2 - Cell performance data for absorbers of different thickness

Thickness	V_{oc} [V]	J_{sc} [mA/cm^2]	FF [%]	R_s	η [%]
Thicker	0.41	29.9	58.5	2.83	7.16
Baseline	0.40	31.3	62.1	1.99	7.73
Thinner	0.38	32.6	61.1	1.90	7.61
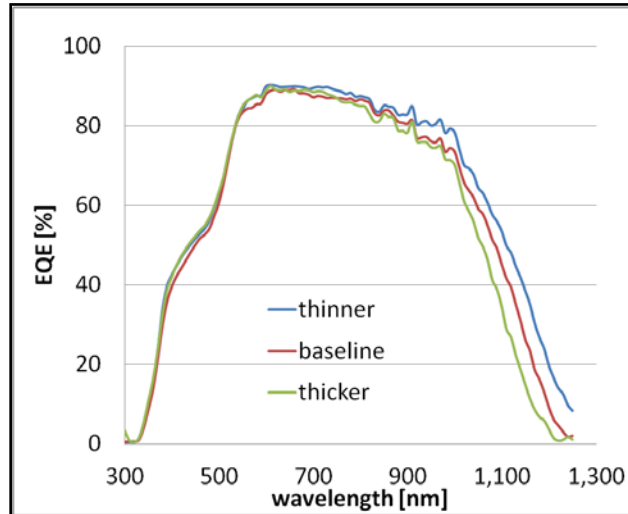
Figure 7 - External quantum efficiency for different absorber layer thickness.

Work continued to understand the formation kinetics of the multi-layer absorber. In order to facilitate the growth of large grains, attempts were made to utilize additive materials to create a low-temperature liquid-phase as a flux agent. To avoid affecting the electronic attributes of the absorbers, only constituent elements were used. While the addition of these elements affect the composition and ratios, the overall ratios were kept within the 0.80-0.95 Cu/(Zn+Sn) and 1.1-1.3 Zn/Sn ratio ranges. The experiment examined two different Cu/Zn+Sn ratios as calculated including both CZTS and the compound materials. In the first case, the CZTS stoichiometry was adjusted such that the final Cu/(Zn+Sn) ratio matched our standard baseline ratio. These devices yielded efficiency on par with comparison CZTS-only baseline samples. In the second case, the mixture was used to change the Cu/Zn+Sn ratio to an overall higher value. The higher ratio material yielded approximately 1% lower cell performance compared to the baseline control devices. More importantly, SEM examination showed no notable change in morphology due to the added compound suggesting that either the addition was insufficient to provide localized liquid phase or the liquid phase assist was insufficient to significantly impact the grain growth.

Another effort to affect and control the film morphology was to include selenium in the compound NPs in hopes of changing the kinetics of sintering. This is related to the all-CZTSe NPs used in the first quarter work. Two compositions were investigated; 30% and 50% Se. Results showed that the grain growth of the films was not greatly affected with either composition. Cell performance was surprisingly unaffected from the baseline performance by this NP composition modification indicating again how wide a process window this NP approach has for the CZTSSe material system.

Cell Shunting

To work toward determining the root cause of the shunting that the cells experience upon grid deposition, we collaborated with NREL researcher Steve Johnston on Drive-Level Infrared Thermography (DLIT), to highlight multiple localized shunt locations on the devices. Interestingly there were shunt spots identified both on/under the grid as well as adjacent to the grid pattern.

993007CA-2_DLITzoom_0p5Vrev_12p6Hz_001
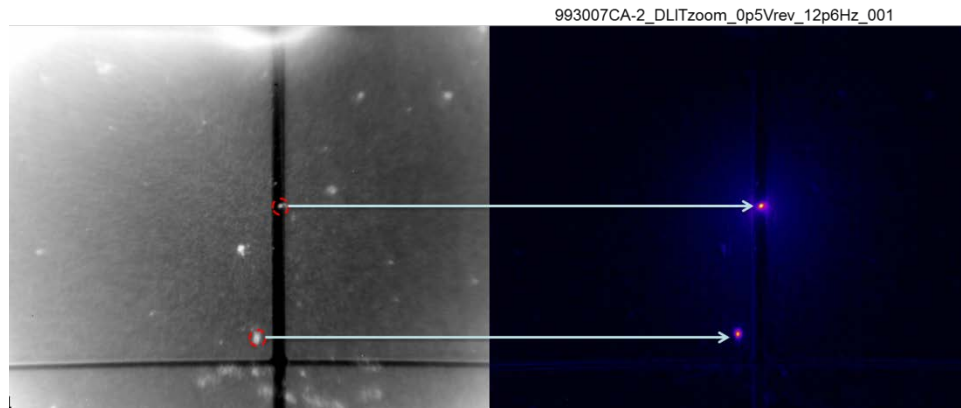
Figure 8 - Drive Level Infrared Thermography (DLIT) picture illustrating shunt points in small-area devices.

Substrate/Back Contact

Molybdenum back contact deposited on metallic diffusion barrier layer has shown significant reactivity with selenium during thermal process. For this reason, our team investigated how modified back contact affects device performance by adjusting sputtering conditions. The results showed that high working pressure and high power density of molybdenum deposition improved device performance, mainly by improving fill factor compared to low working pressure and power density. Moreover, the thickness of the molybdenum disulfide ($MoSe_2$) layer was reduced approximately 50%. This may be attributed to either higher density due to higher power density or to an increase in oxygen concentration from the background sputtering environment as O_2 is known to incorporate more readily into the deposited films at higher pressures. Based on these results a study was launched to investigate the effect of Mo reactivity to selenium with varying levels of O_2 incorporated in the Mo during the sputtering process. The desire was to change the reactivity without significantly affecting the conductivity of the back contact layer. To accomplish this Mo layers were deposited with low percentage levels of O_2 to effectively "dope" the Mo with O_2. All O_2 concentrations investigated, even as low as 1% O_2, showed notable reduction in the thickness of $MoSe_2$ formed during reactive anneal. Cell performance was unaffected by the modified Mo deposition process, thus providing a viable route for protection against over-selenizing of the back contact. Alternatively we evaluated the replacement of Mo by a high work function metal back contact (i.e., tungsten) but encountered a significant delamination issue during thermal process which dissuaded further investigation of that material.

Absorber Process Scalability

The manufacturability of CZTSe solar cells is a critical issue in the near future. Therefore, a significant effort was focused on the development of alternative thermal processing of the printed layers with fast and controllable ramp and soak profiles. Various conditions have been investigated, such as ramp rate, temperature, ambient selenium concentration, and dwell time. In general, a fast ramp rate and relatively high temperature ($> 550^{o}C$) caused significant shunting problems stemming from voids between grains. On the other hand, slow ramp rate prevented severe shunting and yielded uniform cell efficiency.
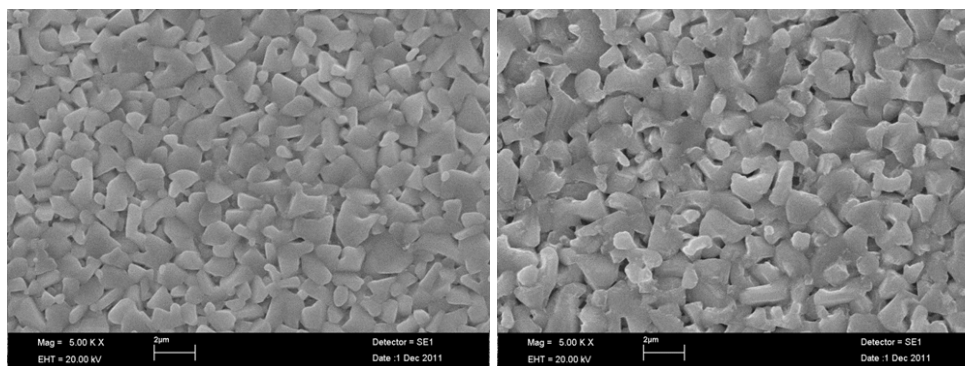

Figure 9 - SEM image of CZTSSe absorber layers annealed at 500°C (left) and 550°C (right) showing significant voids between grains for the higher temperature processed layer.

Increasing the selenium concentration during the anneal process improved cell efficiency and uniformity across the sample. Further investigation in the third quarter was done to understand whether the concentration of the Se or the timing of its introduction and removal in the anneal process was the main driver of this improvement.

Quarter 3

In quarter 3 of the project, the Solexant NP synthesis group continued work on scaling of the NP synthesis and ink process toward the eventual goal of 10-meters of wide web printed material, planned for completion in the final quarter of the project. Meanwhile the process and device group continued to improve small-area cell efficiency to 10%, and to develop larger-area cells to be incorporated into 50mmx50mm mini-modules. The cell efficiency effort included work in eliminating the tri-layer morphology that is typical of Solexant's current reactive anneal process. As this tri-layer is understood to be a materials and process-related issue, ink, printed-layer and selenization processes were explored to solve this issue.

NP and Ink Development

Toward solving the tri-layer absorber morphology, alternative materials were investigated to understand their impact on the tri-layer formation. This approach included the addition of different materials into the baseline CZTS ink, printing of layers of different composition beneath, between and on top of baseline CZTS printed layers, and complete layers of alternative materials. The alternative materials investigated include binary sulfides and selenides as well as CZTSe NP inks.

The most significant departure from baseline quarternary CZTS NP inks was the investigation of all-binary layers. For this, binary sulfides of Cu, Zn and Sn were synthesized and subsequently

13

mixed in an ink targeting typical ratios of Cu/(Zn+Sn) of 0.80 and Zn/Sn of 1.20. Using our baseline selenization process conditions, these binary composition layers did not exhibit grain growth but rather looked quite amorphous under cross-sectional SEM. Upon using more aggressive selenization conditions, some grain growth was evident but all cells made on the samples from various selenization conditions investigated gave minimal photoresponse.
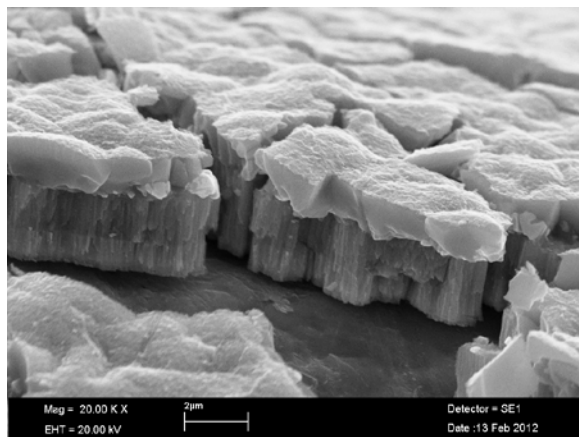
Figure 10 - CZTSe absorber formed by selenization of binary sulfides shows non-crystalline layer.

In addition to investigating different composition materials, several different surfactants used in the NP synthesis process were investigated including dodecylamine and dodecanethiol. To understand the impact of ligands to the tri-layer formation, ligand exchange was performed using pyridine and short-chain alkylamines to reduce the ligand chain length in hopes of promoting the loss of organics at lower temperatures. While these alternative surfactants and ligands did result in a reduced thermogravimetric analysis (TGA) weight loss, indicating that there is less organics on the particles (Figure 11), all efforts using these alternatives produced absorber layers of similar tri-layer morphology and similar, or lower, performing devices.
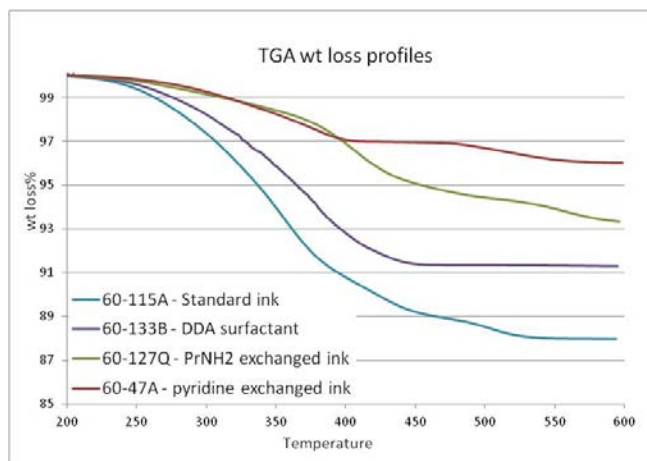
Figure 11 - TGA weight loss profiles of CZTS NPs with alternative surfactants and ligands.

In addition to the surfactants and ligand exchanges noted above, we investigated ligands that decompose more easily such as tert-thiols as they have weaker C-S bonds and release alkyl chain. Multiple trials using these alternatives demonstrated a lack of NP solubility and thus were dropped.

14

Work continued on ink viscosity modification to achieve a higher viscosity ink that is suitable to printing on our wide-web Pilot Line print tool. One additive that was previously investigated and found to not inhibit the cell performance was ethyl cellulose (EC). Based on that earlier work we pursued further development of the now higher-efficiency cells with the EC additive. In this investigation it was discovered that the residual isopropyl alcohol (IPA) that is present in our standard inks, originating from a precipitation step following synthesis, affected the EC's ability to increase viscosity. Once identified, it was easy to adjust the formulation to have more consistent IPA concentration and thereby get repeatable results. With the EC we achieved viscosities up to 7 cP (at 750 sec^{-1}), an acceptable range for our Pilot Line print tool. Print trials were successful in demonstrating suitability of this ink formulation to pilot printing and results of the full-width printing effort are described in the quarter 4 section of this report.

Films/Devices

Continued refinement to our absorber layer and thermal processing yielded improved efficiency devices in quarter 3. Solexant in-house measurement under AM1.5G conditions (referenced to NREL-calibrated cells) gave performance up to 10.22% as shown below. This and two other devices were submitted for NREL measurement and were confirmed to have met the efficiency criteria to meet the 10% small-area cell deliverable.
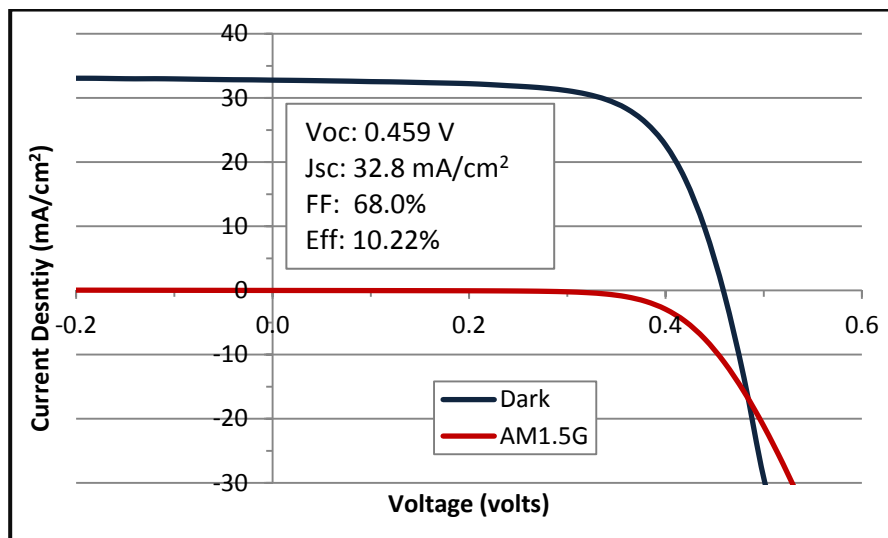

Figure 12 - Solexant in-house measurement of a 10.2% device submitted to NREL as part of the 10% deliverable requirement.

Solexant

CZTS Cell

Device ID: 993013HD-9
Mar 12, 2012 11:10
Spectrum: ASTM G173 global

Device Temperature: 25.0 ± 0.5 °C
Device Area: 0.2439 cm^2
Irradiance: 1000.0 W/m^2

X25 IV System
PV Performance Characterization Team

V_{oc} = 0.4568 V
I_{sc} = 7.9556 mA
J_{sc} = 32.620 mA/cm^2
Fill Factor = 66.08 %

I_{max} = 6.8695 mA
V_{max} = 0.3496 V
P_{max} = 2.4017 mW
Efficiency = 9.85 %

10 min light soak; 5 min cool down
accidental scratch on cell

Figure 13 - NREL measurement of a device submitted as part of the 10% cell deliverable requirement.

Shunting

As discussed earlier in this report, in the development of higher efficiency and larger area cells it became apparent that shunting was occurring on a frequent basis after evaporated grid contacts were deposited. Solexant small area cells are small enough that a grid is not required for I-V measurement and so this phenomenon did not present itself until evaporated grids were deposited on cells destined for NREL I-V measurement. The collaborative effort between Solexant and NREL showed shunts present (Figure 8 above) and further study was done at NREL to work toward an understanding of the root cause of these shunts. NREL used the samples analyzed by Drive Level Infrared Thermography to pinpoint the shunts and teamed up with the Electron Microscopy team to image those offending areas by SEM, FIB-SEM and cross-sectional EDS. With the EDS, NREL was able to identify the source of the defect (Figure 14), namely what appears to be a pinhole in the barrier layer that allowed selenium to react during selenization with the stainless steel substrate and thereby grow a foreign FeSe$_x$ "wire" up through the overlying CZTSSe absorber layer. Fe reacts very favorably with Se to form FeSe$_x$ such that the "wire" was able to grow through the entire absorber layer thickness and present itself to the overlying CdS and TCO layers, thereby creating the offending shunt.

16
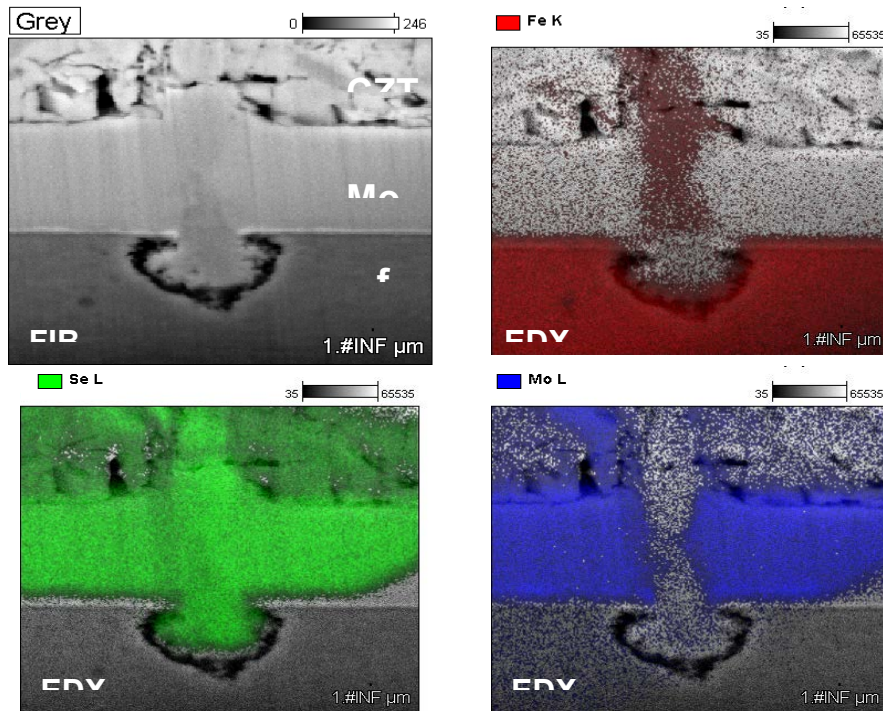
Figure 14 - EDX of CZTS shunting defect after FIB cut.

What also became evident through this FIB-SEM analysis is that there are some areas of barrier layer failure where the Se reaction is insufficient to grow an $FeSe_x$ "wire" but clearly adequate to disrupt the absorber layer growth above (Figure 15). These results illustrate a clear need to reduce these barrier layer pinholes by improved substrate cleaning and reduced exposure to airborne particles before deposition and improving the barrier layer film density. Steps were taken to improve the cleaning and QC procedure as well as the cleanliness of the barrier layer deposition tool chamber and surrounding area resulting in a lower density of the $FeSe_x$ wires. Unfortunately during the course of this project, we were not able to completely eliminate these defects which pose a significant challenge for larger-area cells. This ongoing challenge resulted in large-area cells (25mmx25mm) being approximately 2% absolute lower than their small-area counterparts.
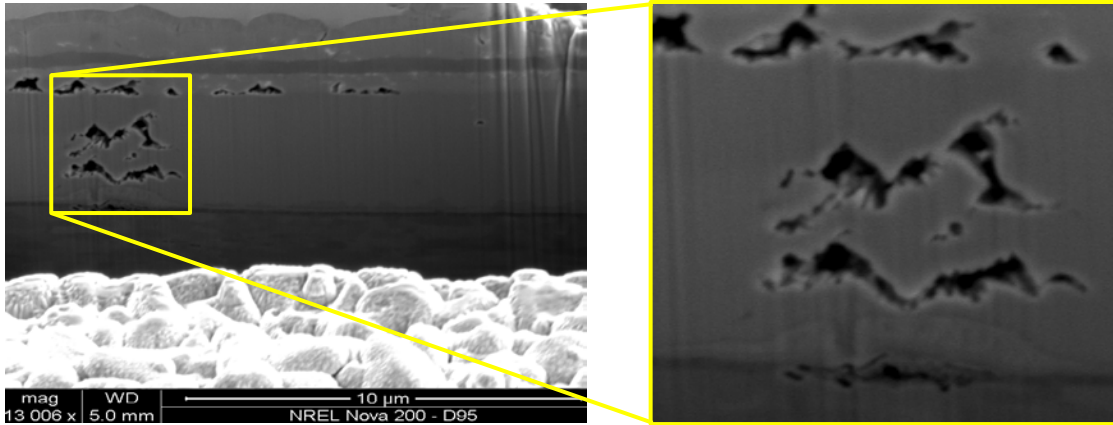
Figure 15 - FIB-SEM micrograph showing less offending defect stemming from barrier layer pinhole.

Several logistical items were put in place during the latter part of the contract Q2 and into the first half of Q3 including scaling of the selenization tooling, scaling of the CBD CdS tooling and process, scaling of the TCO tooling and process and fabrication of new evaporation masks for large-area cell grid formation. Additionally the grid process was transferred to a new electron-beam tool in order to ensure sufficiently thick grid aluminum layers for the increase cell size. All of these changes required not only tooling changes but as well a significant effort in process development. Large-area cells were fabricated and large-area cell efficiencies have improved, breaching 8% in the final quarter of the project.
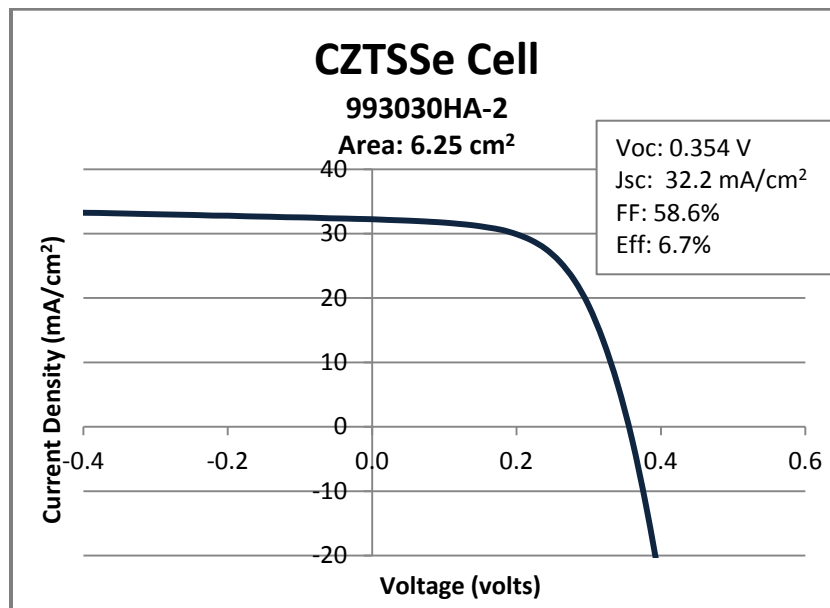
Figure 16 - Current Density vs. Voltage of Recent Large-area (25mmx25mm) Cell.

RTP selenization of the CZTS layers continued to make strides in cell efficiency, producing cells typically between 7% and 8% by the end of quarter 3, with the best cells being between 8% and 8.5%. As mentioned in an earlier report, the uniformity of cell response across the 1"x1" coupon is superior to the baseline tube-furnace process which suggests it may be more suitable for

larger-area cell fabrication. Unfortunately the layers formed by RTP selenization also suffer from the tri-layer absorber morphology and therefore are limited.

Final Quarter Development Details

Quarter 4

Absorber Morphology Improvement

As part of the process of attempting to control the tri-layer morphology of Solexant absorber layers, the effect of the drying temperature on final device CZTSSe film morphology was investigated. It had been noted early in the project that drying a printed film at high temperature (375°C vs. the 300°C baseline) resulted in films that exhibited poor grain growth. Exploration of the intermediate region, namely 350°C, produced an interesting device morphology variant as shown below (Baseline on left, 350°C drying on right).
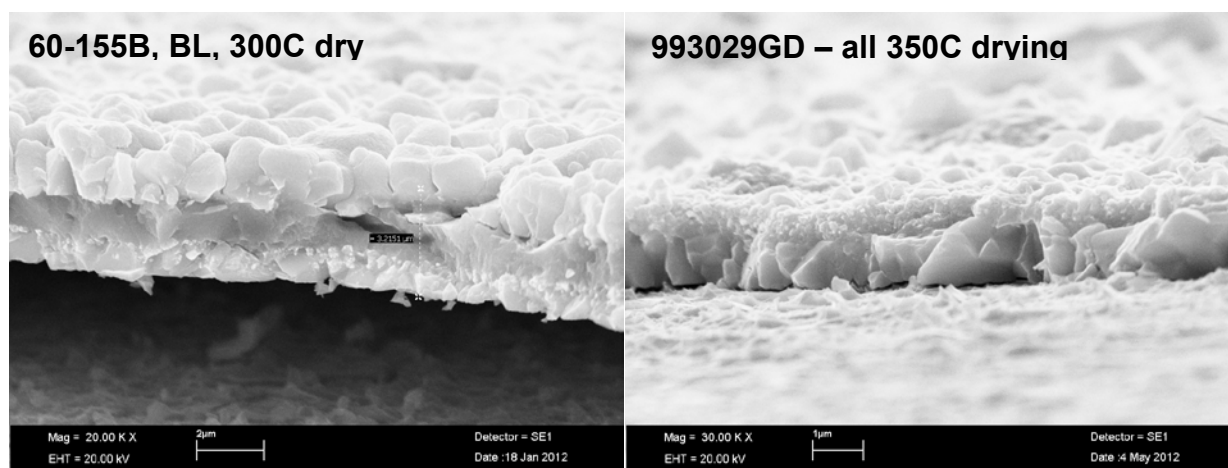

Figure 17 - Cross-section SEM showing effect of drying temperature (300°C left, 350°C right) on absorber morphology.

The presence of the smaller grain material as a top (rather than middle) layer presented the chance to remove the material by chemical or physical etching. Plasma treatment proved the most effective at causing the upper layer to delaminate from the lower large grained material. However, further experimentation with drying temperature and time in the 300-375°C range, 1-3 minutes demonstrated variable responses due to reproducibility issues and so this project was not pursued extensively.

Wide Web Printing/Cell Fabrication

As part of the subcontract requirement, CZTS ink was printed at >10 m length on Solexant's 750 mm wide Pilot Line slot-die web printing tool. This required the development of a more viscous CZTS formulation. Based on some earlier experimental trials, ethylcellulose was chosen as the polymer of choice to increase the viscosity. Several R&D trials demonstrated that this polymer was effective in viscosity enhancement with moderate compromise in cell efficiency. However the reduced efficiency was approximately 1-2% absolute, so not enough to compromise the 4% deliverable. As a starting point for wide-web printing, test runs were performed on a die shimmed to 190 mm width using inks of various viscosities to determine the appropriate viscosity and web-speeds for printing. The table below summarizes the results.

Table 3 - Results of ink printing trials on pilot slot die (ND thickness = not determined)

| Run#	Ink visc. (cP)	webspeed (mpm)	flow rate (mL/min)	print observations	SEM thickness* mid-film (nm)
1	2.6	0.5	2.2	no stable bead	ND
2	2.6	1	2.2	no stable bead	ND
3	2.6	2	2.2	stable bead, good witness line	ND
4	4.7	0.5	2.2	no stable bead	ND
5	4.7	1	2.2	stable bead, some witness drips	270
6	6.8	0.5	2.2	no stable bead	ND
7	6.8	1	2.2	stable bead, good witness line	235
8	6.8	1	3.3	no stable bead	400
9	6.8	1	3	likely stable bead, some witness drip	390
					*after drying 350C, 1min

From these results it was extrapolated that a web speed of 1.5 m/min and a flow rate of 3.9 mL/min would be appropriate to maintain a stable ink bead at the slot-die to web interface at full width. When moving to the 750 mm web format, several test prints were made to confirm the print stability before commencing the 10 m print. A photo is shown below of the first "on print" run at full wide, where the printed layer (the first of four prints) is seen to emerge over the roller from the slot-die printing head.
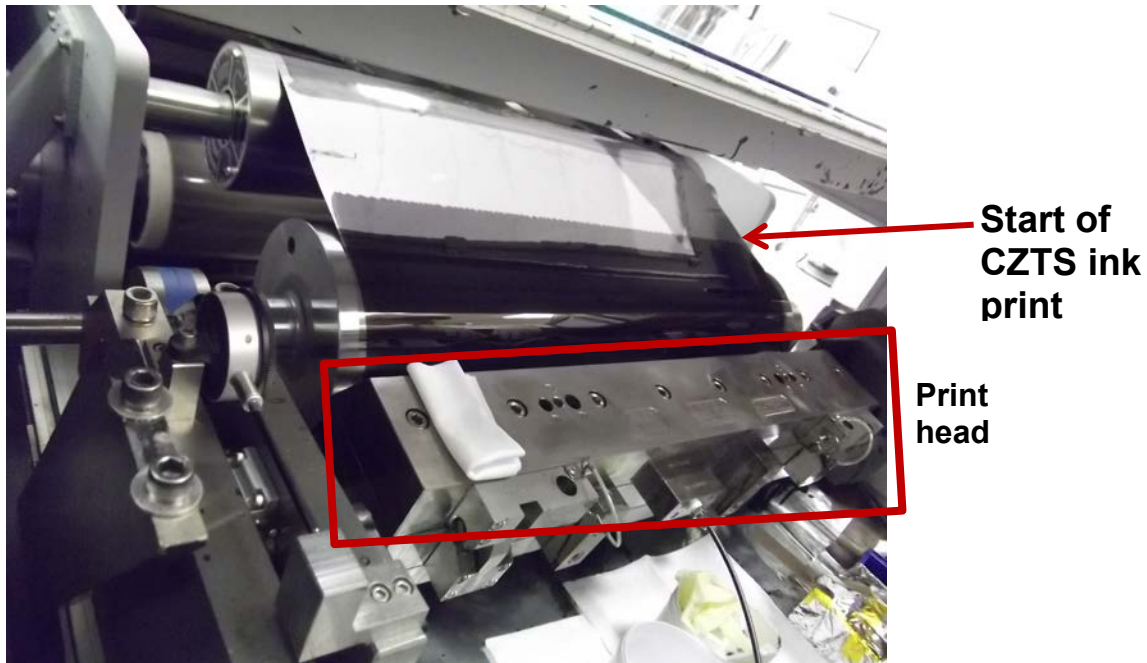
A diagram of the print web and sampling for the device performance evaluation is shown below.

4-Print End 29.7m

4-Print Start

Tail
L~2m

Active
Print 4P

Test Prints

1P

Test Prints

1P

Leader
L~17.1m

Outside
wrap

Web
Core

**D1249-287-XX Samples
Cut In-Situ**
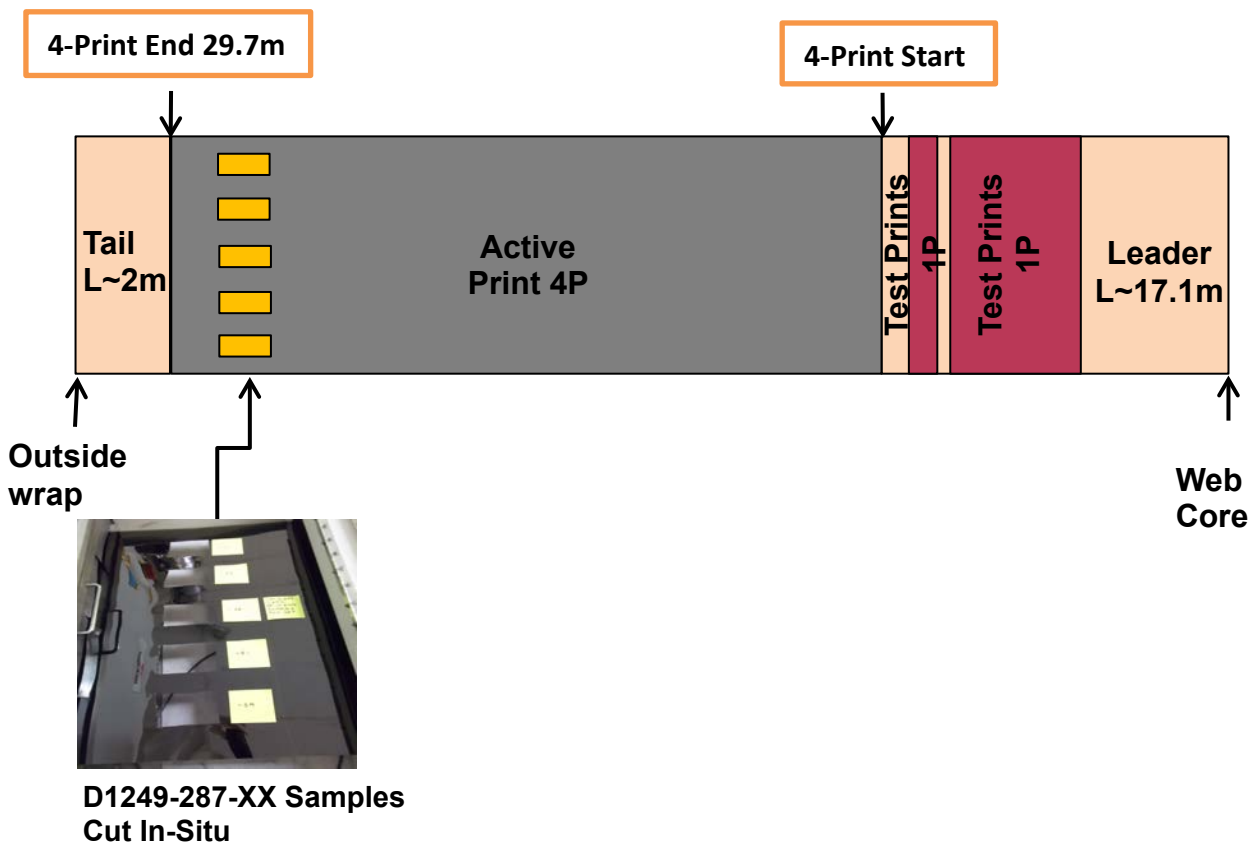
The selected cross-web print samples were processed through devices using the R&D selenization and device completion process line. The device results obtained at Solexant are summarized below. The sampling numbers are of the format D1249 (internal lot number) - 287 (decimeters from beginning of web) – xxY (xx = centimeters from edge of web, Y = letter code for internal tracking of 1"x1" substrate experiments).

Table 4 - Cell efficiency results from 10-meter printed web trial

sample	Voc (V)	Jsc (mA/cr	Fill Factor	Avg Eff 9/9 cells (%)	eff. best cell (%)
D1249-287-11B	0.405	28.9	54.5	6.36	6.70
D1249-287-24B	0.397	29.2	50.1	5.82	6.34
D1249-287-38C	0.324	27.5	45.4	4.58	5.43
D1249-287-51B	0.400	29.2	51.6	6.03	6.46
D1249-287-64B	0.332	30.5	45.0	4.73	6.10

As can be surmised from the data above, cross-web efficiency was generally good and exceeded the deliverable requirement of 4% efficiency. Some 1"x1" samples (which are photolithography-isolated into nine pixels of 0.25 cm^2 area each) contained "dead" cells that bring the average efficiency down well below the best devices. This is due to substrate, handling and/or post-printing process issues that result in device shunting rather than an issue with the printing process itself.

Films/Devices – The role of NaF for small area device performance via rapid thermal process (RTP)

Incorporating sodium fluoride (NaF) plays a critical role to enhance device performance. Capacitance-Voltage data suggested that NaF increases carrier concentration significantly up to one order of magnitude and decreases depletion width, resulting in increased open circuit voltage. In addition, NaF increases the degree of selenization, resulting in a lowering of the band gap (as determined from external quantum efficiency (EQE) data) and significant increase grain size as shown in Figure 18 below. As a result, we achieved our best RTP-based small-area cell efficiency of 9.79%. A notable characteristic of samples processed by the rapid thermal process was good lateral uniformity of device performance of the 9 small-area cells on standard 1"x1"coupons, which suggested it would be more suitable for large area cells (25mmx25mm).
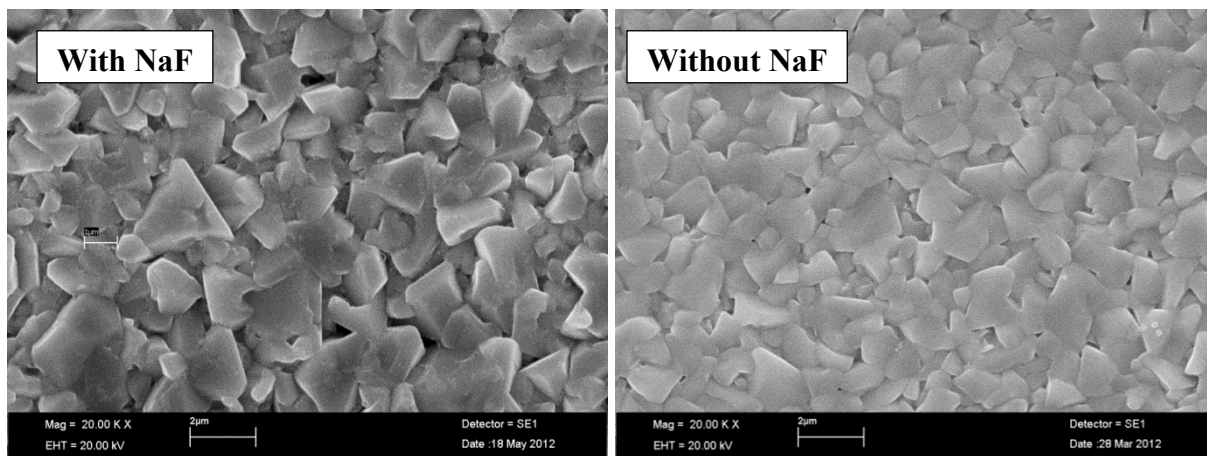

Figure 18 - SEM images of CZTSSe crystals grown with and without NaF additive.

Films/Devices - Large area cells

Significant work was focused on larger area cells (25mm x 25mm) in order to achieve the subcontract deliverable of 7% efficient 50mmx50mm mini-module. As discussed above, shunt behavior stemming from substrate defects has been a major obstacle to achieving higher efficiency in the large area cells required for mini-module fabrication. We pursued several avenues to address this challenge, including alternate substrate foils, different substrate barrier materials and deposition process conditions, and high-resistivity transparent (HRT) layers on the top of the device to mitigate the shunts.

The shunts are created when pinholes in the substrate barrier allow Se to react with the Fe in our baseline stainless steel foil substrates, creating $FeSe_x$ "wire" protrusions during the selenization process. Two alternative substrate foils, Mo and Ti, were explored based on the theory that their lack of Fe composition would remove the source of the shunt material. We found that both Mo and Ti foils still produced defects during device selenization, but the defect source and nature were somewhat different from baseline.

The Mo foil substrate still contained a non-ideal physical defect density. The predominant type of defect showed no Fe and is theorized to result from barrier layer imperfections allowing Se to access the Mo foil and create $MoSe_2$ protrusions. A limited number of $FeSe_x$-based defects were also present, believed to stem from Fe inclusions embedded in the foil during rolling where

highly polished stainless steel rollers are used. However, in spite of this some Mo foil devices showed a notable improvement in shunt resistance compared to our baseline stainless steel device performance, allowing us to achieve up to 7.52% on large area devices. From these results it is believed that the predominant defects must be less conductive than the stainless steel defect analogs.

Ti foil-based devices still showed a high density of absorber layer defects, but $FeSe_x$ wires were eliminated. The defects appear as eruptions up from below the absorber layer and their root cause remains uncertain. No foreign materials were detected by EDS. Although shunting was decreased compared to baseline SS foil-based devices, the Ti foil devices typically performed at a lower level than those on Mo foil. The best Ti foil device yielded 6.95%.
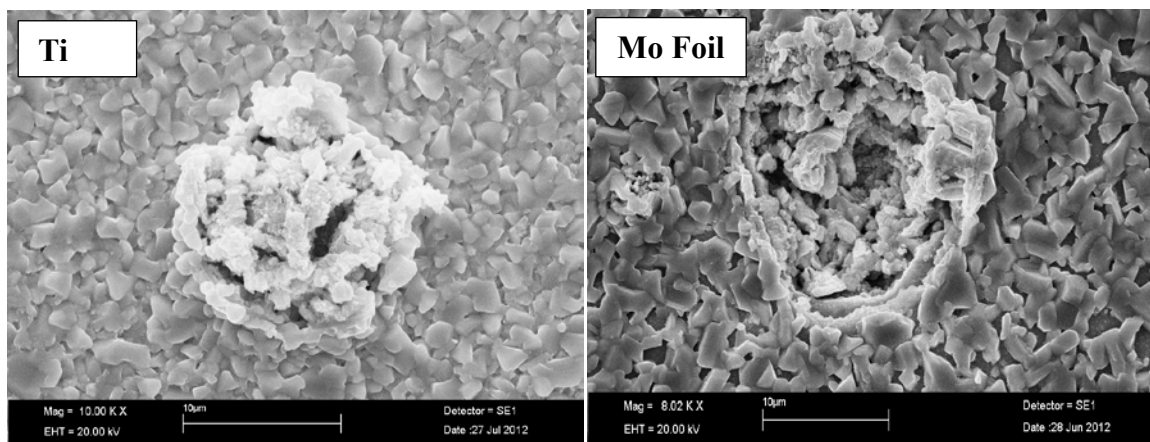

Figure 19 - Typical defects for Ti and Mo foil devices.

Our original baseline substrate barrier layer was a metallic bilayer. We investigated TiN in single and multi-stack configurations using different deposition conditions as a potential improved barrier. However, while we were able to achieve comparable device performance, the TiN combinations did not impede defect formation nor give improved efficiency. In particular, the TiN barrier seemed to limit V_{oc} (< 0.35V) compared to typical V_{oc} (~0.38-0.4V) of devices on baseline barrier layers.

We have incorporated NaF to enhance large-area device performance. Solexant in-house measurement under AM1.5G conditions has shown performance up to 8.4% by RTP selenization. This suggests a promising route to achieve the 7% mini-module. However, this result was inconsistent using RTP and was not replicated using tube furnace selenization. The source of inconsistency is not certain, but variation in the evaporated NaF layer thickness is a prime suspect.

Figure 20 - Best large-area (6.25cm^2) cell efficiency achieved

Table 5 - Best large-area cell efficiencies for different substrate, barrier layer and treatment combinations

Substrate	barrier layer	Treatment	V_{oc} [V]	J_{sc} [mA/cm^2]	FF [%]	Eff [%]
SS	Baseline	NaF	0.405	34.5	60.0	8.38
Mo	Ti/TiN	none	0.390	32.4	59.3	7.52
Ti	none	none	0.381	30.4	59.9	6.95

As an alternative approach for mitigating shunting, we attempted to block the shunt pathways using HRT layers placed between the CdS and TCO layer. We explored i-ZnO (thicker than baseline), Ga$_2$O$_3$ and LiF. Of these, the only improvement came from thicker i-ZnO on otherwise baseline RTP devices. As hoped the thicker i-ZnO layer notably improved the shunt resistance without compromising other device parameters. Interestingly, annealing process significantly improved both shunt resistance and diode quality factor as shown in dark I-V (Fig 21).
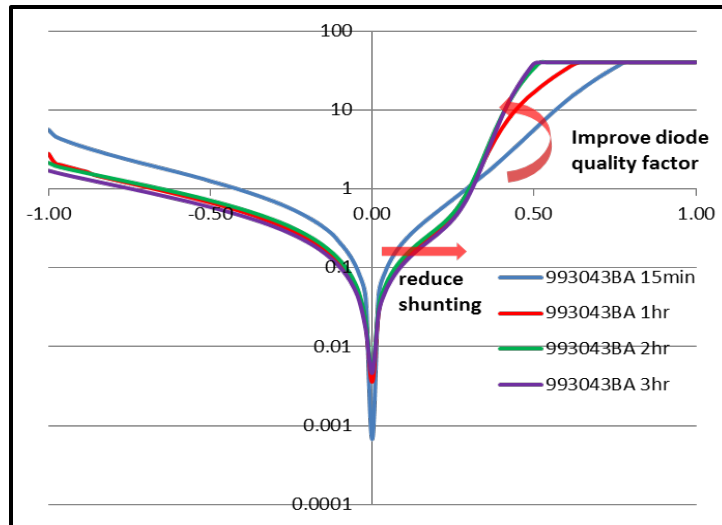
Figure 21 - Improvement in dark IV characteristic with anneal for thicker IZO device.

The effort on mini-module fabrication resulted in the achievement of a 7.1% mini-module consisting of four 25mm x 25mm cells connected in series, which included the champion 8.3% large-area cell and is shown in Figure 22.

Figure 22 - Champion 7.1% efficiency mini-module with 25 cm^2 area.

The I-V chart of the champion mini-module is shown in Figure 23 below.
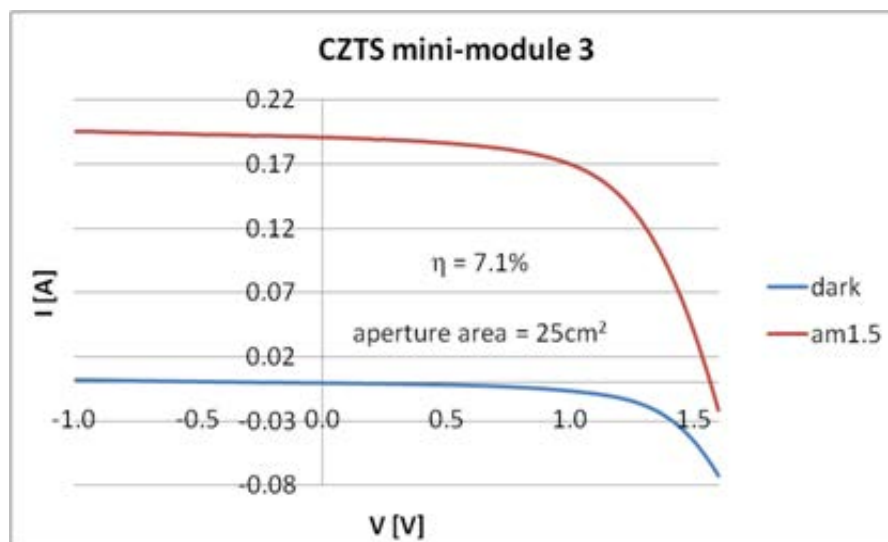
Figure 23 - I-V of 7.1% (internal measurement) champion efficiency mini-module, 25 cm[2].

4 Conclusion

Solexant has successfully completed a research sub-contract to develop high-efficiency $CuZnSnS_xSe_{2-x}$ (CZTSSe) solar cells. CZTS has come of interest because of its similarity to $CuInGaSe_2$ (CIGS), the current thin-film efficiency world record holder, and the relative earth abundance of its constituents, which provide a potentially lower cost alternative to CIGS.

The high vapor pressure of sulfur has proven a challenge in co-evaporation processes, the process which for CIGS has yielded the highest efficiency solar cells. However some early success has been reported by groups using non-vacuum techniques to prepare absorbers. These include solution-based techniques as well as nanoparticle (NP) approaches. Solexant's principle technology platform uses non-vacuum NP-based solutions/inks on flexible metal foil as the foundation for solar cells. It is with this NP-on-foil approach that Solexant pursued under this sub-contract the development of CZTS solar cell devices.

Over the course of this sub-contract, the effort began on fundamental nanoparticle (NP) chemistries for forming the desired composition nanoparticles and formulating a suitable ink for printing. Additionally the fundamental building blocks of both front and back contacts had to be established. Once established, solar cell device work began in earnest, with small modifications to the NP synthesis and ink to address specific issues as they were encountered.

In the second quarter of the subcontract, work continued on improving the solar cell efficiency using the baseline structure and selenization processes established in the early months of the program. As part of this effort work focused on the back contact and absorber layers in particular, in an effort to improve series resistance and adhesion/reliability of the molybdenum back contact and to improve the crystal growth of the absorber layer. Progress was made in both areas while at the same time the thermal formation process was modified to achieve a more scalable, shorter overall process time anneal.

26

The third quarter of the project focused on four primary areas, namely scaling of the NP synthesis and ink process, scaling of the device area from 0.25 to 6.25cm^2, identification of the source of the shunt defects, and elimination of the tri-layer absorber morphology. The successful scaling of the ink process put in place the pieces needed to print several continuous meters of web on Solexant's pilot line printing tool in the following quarter. In collaboration with NREL, the base characteristics of the shunt defects were identified, providing a framework for the fourth quarter efforts to eliminate the defects. Much effort was expended in scaling the tooling and device fabrication processes to large area cells, resulting in 6.25cm^2 cells up to 6.7% efficiency in the third quarter. Meanwhile, ongoing work to improve small-area device processing yielded champion efficiencies meeting the 10% efficiency deliverable requirement.

During the final quarter of the grant, we demonstrated >10 meters successful printing of the NP ink on Solexant's pilot line printing tool. Devices made from areas sampled across the web yielded devices with over 6% efficiency. Meanwhile, variation of ink drying on the smaller scale produced some instances of bilayer absorber morphology. However, the response was variable and this avenue was not pursued further.

Incorporation of NaF in the absorber produced higher efficiency devices in both small and large area devices when processed by RTP selenization, including the champion 8.3% large-area cell. While the results with NaF were inconsistent, they suggest a promising future avenue for development. Large area devices were still limited by shunting, though, so much effort was expended on different approaches to solve the shunting problem. Different foils, barriers and HRT layers were developed and tested, however, no one avenue showed a consistent and complete solution. Some Mo foil samples created devices with notably improved shunt resistance and for RTP devices a thicker i-ZnO HRT layer also reduced shunt behavior. Combinations of these approaches produced large area devices that, assembled together, gave 25x100mm (25cm^2) mini-module efficiency up to 7.1%.

Acknowledgements